Journal of Power Sources 196 (2011) 3633–3639

Contents lists available at ScienceDirect

Journal of Power Sources

journal homepage: www.elsevier.com/locate/jpowsour

A modified carbothermal reduction method for preparation of high-performance nano-scale core/shell Cu_6Sn_5 alloy anodes in Li-ion batteries

Wangjun Cui, Fei Wang, Jie Wang, Haijing Liu, Congxiao Wang, Yongyao Xia*

Department of Chemistry and Shanghai Key Laboratory of Molecular Catalysis and Innovative Materials, Institute of New Energy, Fudan University, Shanghai 200433, People's Republic of China

ARTICLE INFO

Article history:
Received 20 September 2010
Received in revised form
16 November 2010
Accepted 10 December 2010
Available online 21 December 2010

Keywords:
Intermetallic compounds
Carbothermal reduction
Hydrophobic powders
Lithium-ion battery

ABSTRACT

Core–shell structured, carbon-coated, nano-scale Cu_6Sn_5 has been prepared by a modified carbothermal reduction method using polymer coated mixed oxides of CuO and SnO_2 as precursors. On heat treatment, the mixture oxides were converted into Cu_6Sn_5 alloy by carbothermal reduction. Simultaneously, the remnants carbon was coated on the surface of the Cu_6Sn_5 particles to form a core–shell structure. Transmission electron microscope (TEM) images demonstrate that the well-coated carbon layer effectively prevents the encapsulated, low melting point alloy from out flowing in a high-temperature treatment process. Core–shell structured, carbon coated Cu_6Sn_5 delivers a reversible capacity of 420 mAh g^{-1} with capacity retention of 80% after 50 cycles. The improvement in the cycling ability can be attributed to the fact that the carbon-shell prevents aggregation and pulverization of nano-sized tin-based alloy particles during charge/discharge cycling.

1. Introduction

Lithium-ion batteries based on graphite anodes have been widely used in various power applications, but their limited capacity of 372 mAh g^{-1}, poor rate performance and safety problems hampered the use of this battery in higher power systems such as hybrid and electric vehicles. In recent years, many efforts have been directed to develop alternative anode materials. Li-alloys, especially Li–Sn, have attracted much attention due to their high-volumetric and mass-energy density and are considered to have the most potential for use in new lithium-ion batteries [1–4].

However, the large volume expansion and contraction that accompanies the lithium alloying/dealloying process is a major drawback that deteriorates the electrochemistry performance of the Sn anode. These volume changes induce severe mechanical strains that severely limit the cycling life of the lithium-alloy electrodes.

The approaches for improving the electrochemical response of these electrodes most reported on are the following: (i) preparing intermetallic compounds (M′M), such as Cu_6Sn_5 [5], InSb [6], and CoSn [7], which consist of an inactive phase M that does not react with lithium and an active phase M that reacts with lithium; (ii) dispersing nano-sized tin-based materials into a carbon matrix or other "zero-structural change" compound matrix; and (iii) constructing core/shell nanostructure materials or preparing carbon-encapsulated hollow tin nanoparticles, in which the carbon shell can effectively accommodate the strain of volume change during Li^+ insertion/extraction. Scrosati's group proposed a nanostructure Sn–C composite with unique stability [8]. Park et al. adopted a titanium reduction method to synthesize the Sn–TiO_2–C system by constructing a TiO_2–C matrix surrounding nano Sn particles [9]. In 2003, for the first time, Oh and co-workers synthesized tin-encapsulated spherical hollow carbon (24 wt% tin) by sol–gel polymerization with tributylphenyltin as the tin source [10]. Zhang et al. used a template-assisted method to prepare similar tin-based anode materials with an active tin content of 74 wt% and an average tin particle diameter of *ca.* 100 nm [11]. More recently, our group reported a carbon-coated, nano-scale Cu_6Sn_5 prepared by an in situ surface polymerization technology. This material integrates the merits of intermetallic compounds and nano-sized anode materials and showed an improved electrochemistry performance [12]. Nevertheless, in such processes, a precursor of tin alloy nanoparticles should be prepared through sodium borohydride reduction and either mechanically milling or electrochemically deposition. Unfortunately, these methods are either costly or complicated to control particle sizes. Furthermore, the nano-scaled tin alloy particles synthesized by these methods often contain some chloric ions and hydroxyl groups adhered to the surface of particles and were difficult to remove completely. These impurities certainly affect the electrochemical performance of the tin alloy anode [13]. As an alternative, the carbothermal reduction method has been developed to synthesize a wide range of materials, includ-

* Corresponding author. Tel.: +86 21 55664177; fax: +86 21 55664177.
E-mail address: yyxia@fudanedu.cn (Y. Xia).

0378-7753/$ – see front matter © 2011 Elsevier B.V. All rights reserved.
doi:10.1016/j.jpowsour.2010.12.025

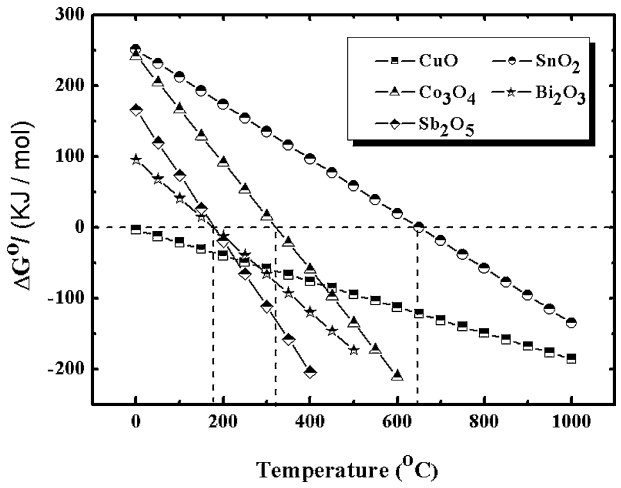

Fig. 1. The relationship of Gibbs free energy of the carbothermal reaction and temperature.

ing polyanions, oxide-based compounds and alloys [14,15]. For example, Hassoun et al. prepared a SnSb/C nano-composite using triphenylantimony and triphenylbutyltin as metal sources [16]. Wang et al. synthesized Cu_6Sn_5-encapsulated carbon microsphere anodes using the carbothermal reduction method [17]. However, the alloy materials reported merely dispersed the metal in the carbon matrix or obtained materials in the size of microns rather than creating a nano-scale core–shell structure. It is worth noting that in the process of carbothermal reduction, the Sn melting point is much lower than the SnO_2 reductive temperature of 650 °C, suggesting that once Sn was reduced from the oxide, it existed as a liquid that makes the alloying process easier. On the other hand, owing to the low melting point of Sn (232 °C), liquid Sn poured off from the outflow during high-temperature treatment. Therefore, preparation of core–shell structured, carbon-coated, Sn-based alloy nanoparticles by carbothermal reduction, which improves the cycling stability of the alloy, is important but very challenging.

In the present work, we introduce a general, effective, modified carbothermal route for synthesis of core–shell, carbon-coated, nano-sized, tin-based materials using the mixed oxides, CuO and SnO_2 as precursors. Nano-scale precursors were used to guarantee homogeneous mixing, and easy reacting. We then introduced the hydrophobic reagent, hexadecyltrimethoxysilane (HTMS), to change the surface condition of the precursor particles and make them disperse well in the organic phase to guarantee that the final product was nano-sized. Carbon is made available in the material through a coating polymer by in situ emulsion polymerization method. The electrochemical performance of these core–shell powders as an anode material for lithium-ion batteries is presented. Micro-structural analyses have also been made, and the relationship between morphological and the electrochemical profile is discussed.

2. Experimental

2.1. Chemicals

Tin chloride hydrate ($SnCl_4{\cdot}5H_2O$, 98%), copper chloride hydrate ($CuCl_2{\cdot}2H_2O$, 99%), sodium borohydride ($NaBH_4$), cetyltrimethyl ammonium bromide (CTAB, 99%), sodium carbonate anhydrous (Na_2CO_3, 99%), formalin solution (37 wt%), m-dihydroxybenzene (Resorcin, 99%) and ethanol were analytical reagents purchased from Shanghai Chemical Company. Hexadecyltrimethoxysilane (HTMS, 85%) was an analytical reagent purchased from Fluka Chemical Company. All chemicals were used as received without further purification. Deionized water was used in all experiments.

2.2. Synthesis of nanocrystalline CuO and SnO_2

Nanocrystalline CuO with a particle size between 5 and 6 nm was synthesized according to previous work [18]. In a typical synthesis, 1.500 g (0.0112 mol) of copper(II) chloride was dissolved in 70 mL of absolute ethanol to form a clear green solution in a 250-mL round-bottom flask. Then 0.0224 mol of sodium hydroxide was dissolved in absolute ethanol and added dropwise to form the copper hydroxide gel. The reaction was then stirred at room temperature for 2 h. During this time, the reaction mixture forms a blue-green gel. After the reaction completed, the solution was filtered and washed with water to remove sodium chloride. The copper hydroxide was then air-dried on a dish, and the copper hydroxide precursor was obtained. To get nanocrystalline CuO, the copper hydroxide powder was then placed in a quartz tube and heated in an argon flow at 250 °C for 15 min. After heat treatment, the copper oxide powder was black. Nanocrystalline SnO_2 was prepared by hydrolyzing a 0.5 M $SnCl_4$ aqueous solution in PTFE-lined autoclaves at 180 °C for 2 h, which was then dried at 80 °C in a ventilated oven [19].

2.3. Synthesis of carbon coated nano-scale Cu_6Sn_5

The procedure for synthesis of nanoscale carbon coated Cu_6Sn_5 is briefly described as an in situ polymerization process. The mixed oxides nanoparticles prepared as described above were used as a starting material. In a general synthesis process, a 1.5 g mixture of stoichiometric oxides powders was dispersed in toluene using a high-power ultrasonic instrument for 30 min. Then, 0.5 mL of hexadecyltrimethoxysilane (HTMS) was added, which modified the surface. The mixture was stirred for 15 min, washed with ethanol, filtered and vacuum dried at 80 °C to obtain hydrophobic powders. The hydrophobic powders were mixed with 250 mL of a solution of deionized water and formalin (1:1, by volume). A homogeneous emulsion was formed after adding CTAB as a surfactant and ultrasonically dispersing for 30 min. As soon as 0.625 g of m-dihydroxybenzene with a 0.16 g Na_2CO_3 initiator was put into the emulsion, a nacarat emulsion appeared. This emulsion, in which the in situ polymerization occurred, was stirred at 80 °C for 12 h. After that, the suspended resol-coated nanoparticles were centrifuged, washed and dried at 80 °C to acquire a raw product. The dried powders were then heated to a reduction temperature, which was identified by differential scanning calorimetry (DSC) analysis with a heating rate of 5 °C min^{-1} in a nitrogen atmosphere, and held for 2 h, where the coating resol layer was carbonized and a crystalline alloy formed. For comparison, Cu_6Sn_5 nanoparticles were synthesized by a sodium borohydride reduction method, which involved reducing a solution of various metal ions with $NaBH_4$ [20].

2.4. Characterization and electrochemistry test

The phase composition of the obtained compounds was characterized by X-ray diffraction (XRD, Bruker D8 X-ray diffractometer) with Cu Ka radiation. The XRD data were analyzed using the software, Material Data Jade 5.0. The pellets of sample powders pressed with KBr were evacuated at 0.01 Pa for 24 h before measuring their in situ IR absorbance spectra on a Bruker Equinox 55 through a cell with CaF_2 windows. Particle morphologies and sizes were characterized with a Philips XL-60 scanning electron microscope and a JOEL JEM2010 transmission electron microscope. Thermo-gravimetric (TG) measurements and differential scanning calorimetry (DSC) was carried out on a Perkin-Elmer TGA 7 thermal

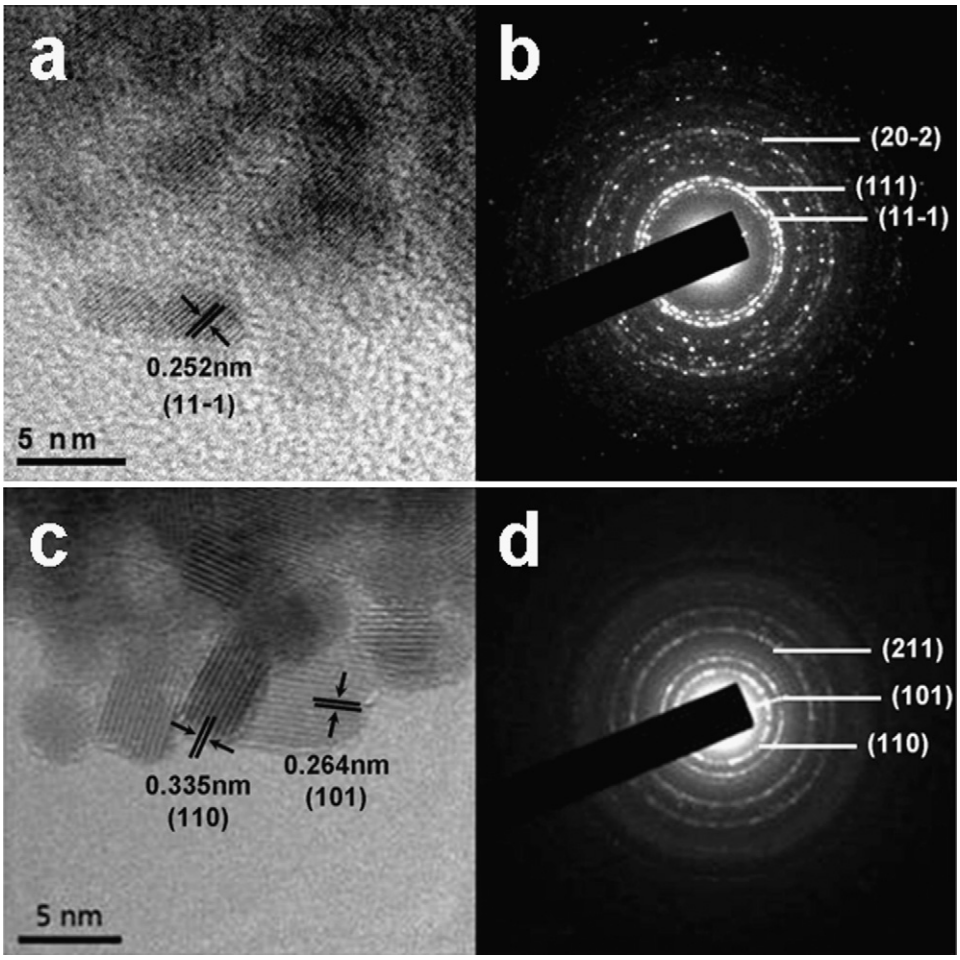

Fig. 2. HRTEM (high resolution transmission electron microscope) of prepared oxides: (a) CuO nano-crystals, (b) CuO nano-crystal SAED pattern, (c) SnO_2 nano-crystals, (d) SnO_2 nano-crystal SAED pattern. The representative lattice spacings are marked with arrows in HRTEM and indexed in SAED images. Uniform crystal nanoparticles with *ca.* 5 nm diameters can be observed.

analyzer at a heating rate of 10 °C min^{-1} in a 40 mL min^{-1} flow of air or nitrogen.

Electrochemical tests were performed in a CR2016-type coin cell. Metallic lithium was used as the negative electrode. The working electrodes were prepared by mixing 80% alloy powders, 10% carbon black, and 10% polyvinylidene fluoride (PVDF) dissolved in *N*-methylpyrrolidinone (NMP). The slurries of the mixture were applied to a Cu foil. After coating, the electrodes were dried at 80 °C for 10 min to remove solvent before pressing. The electrodes were cut into sheets 1 cm^2 in area, vacuum-dried at 100 °C for 24 h and weighed before assembly. The typical mass load of the active material was about 5 mg cm^{-2}. The cell assembly was operated in a glove box (model 100G, MBraun, Germany) filled with pure argon. The electrolyte solution was 1 M $LiPF_6$/ethylene carbonate (EC)/diethyl carbonate (DMC)/ethyl methyl carbonate (EMC) (1:1:1, by volume). The cells were assembled with as-prepared cathodes, lithium metal anodes, and separators made of a Celgard 2300 film. Charge–discharge experiments were performed at a constant current density of 100 mA g^{-1} between 0.0 V and 2.0 V using a LAND CT2001A Battery Cycler (Wuhan, China). The cells were cycled with lithium insertion into the alloy electrode referred to as discharge and extraction as charge.

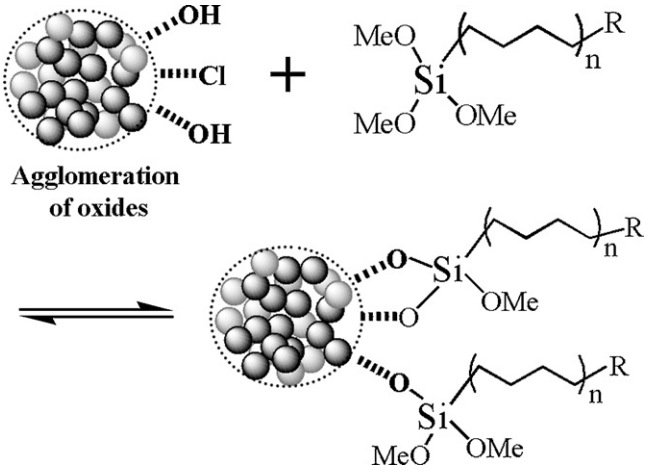

Fig. 3. Conceptual diagrams describing the surface modification mechanism.

3. Results and discussion

3.1. Thermodynamic consideration of carbothermal reduction

For most metal oxides, carbothermal reductions typically occur according to the following reaction:

$$MO_X + C \rightarrow M + xCO^{\uparrow}, \quad (1)$$

where the metal element is denoted as M. The reduction difficulty for a particular metal oxide depends on the affinity of the metal to combine with the oxide lattice. This is characterized by the Gibbs

free energy, ΔG, of the reaction. The reduction temperature can be approximated with thermodynamic data according to the following equation:

$$T \approx \frac{\Delta H - \Delta G}{\Delta S}, \quad (2)$$

where ΔH, ΔG and ΔS represent enthalpy, Gibbs free energy and entropy of the reaction (1), respectively. Fig. 1 gives the Gibbs free energy diagrams that describe the thermodynamic relationship between the free energy of the oxide reductive reaction and temperature. Theoretically, carbothermal reduction reactions will take place at the temperature where ΔG equals zero [14,21]. In Fig. 1, five regular metal oxides were chosen as examples. The reduction temperatures of CuO, SnO_2, Co_3O_4, Bi_2O_3 and Sb_2O_5 can easily be found in the diagram. For example, 190 °C, 320 °C and 650 °C are the reduction temperatures for Sb_2O_5, Co_3O_4 and SnO_2, respectively. However, in most situations, the practical reduction temperature, which is affected by both kinetics and carbon resources, should be confirmed by differential scanning calorimetry (DSC) analysis, as was done in this work.

3.2. Characterization of the synthesis procedure of Cu_6Sn_5/carbon composite

To prepare the Cu_6Sn_5/carbon composite, nanosized CuO and SnO_2 were prepared as precursors according to the reported work [18,19]. The particle sizes of nanocrystalline CuO and SnO_2 were characterized by HRTEM (high resolution transmission electron microscope), as seen in Fig. 2.

The composites are composed of small nanocrystallines. The primary particle size of the obtained oxides was *ca.* 5 nm, as shown in Fig. 2a and c. The HRTEM image of the nano-CuO in Fig. 2a shows clear and continuous lattice fringe images. The distance between neighboring fringes is 0.252 nm, close to the (1 1 −1) lattice spacing in a monoclinic Tenorite-type lattice (C2/c, JCPDS card no. 48-1548). The selected area electron diffraction (SAED) pattern shown in Fig. 2b indicates clear diffraction rings that represent the (1 1 −1), (1 1 1), and (2 0 −2) planes of CuO. Additionally, the image of the hydrothermally prepared SnO_2 particles, with an average size of *ca.* 5 nm, is shown in Fig. 2c. The tetragonal-type SnO_2 (*P*42/*mnm*, JCPDS card no. 77-0448) shows 0.335 nm and 0.264 nm distances between neighboring fringes, which correspond to the lattice spacings of the (1 1 0) and (1 0 1) planes. The SAED pattern shown in Fig. 2d shows several sharp rings, which correspond to the (1 1 0), (1 0 1), and (2 1 1) planes of the rutile crystalline structure of SnO_2.

For preparing a uniform, core–shell, carbon-coated, nano-scale Cu_6Sn_5 alloy, the obtained nano-oxide particles were dispersed in toluene using a high power ultrasonic instrument, followed by hydrophobic treatment with hexadecyltrimethoxysilane (HTMS). They can be "grafted" onto the oxide particles to keep them stable with metal–O–Si bonds, while the alkyl chains pointing to the outside make the particles disperse well in the organic phase (the modification mechanism is shown in Fig. 3). This is a key point to guarantee that polymerization occurs on a single particle surface and ensure that the polymer layer firmly coats the grains. Additionally, trace amounts of hexadecyltrimethoxy–silane cannot produce much silicate compounds during the subsequent heat treatment. The IR spectrometry of a CuO/SnO_2 mixture, HTMS modified CuO/SnO_2 mixture and pure HTMS shown in Fig. 4 presents first-hand evidence for the modified effect of HTMS. Comparing the IR spectra of the modified CuO/SnO_2 mixture and unmodified oxide mixture reveals that alkyl chains are grafted to the oxides' surfaces after the metal–O–Si bonds are formed (C–H vibrations: 2875, 1460, and 1250 cm^{-1}; Si–O vibration: from 1160 to 1190 cm^{-1}) [19]. Sn–O–Sn stretching at 667 cm^{-1} inside SnO_2 particles remained unchanged after the surface was modified, while a slight move of

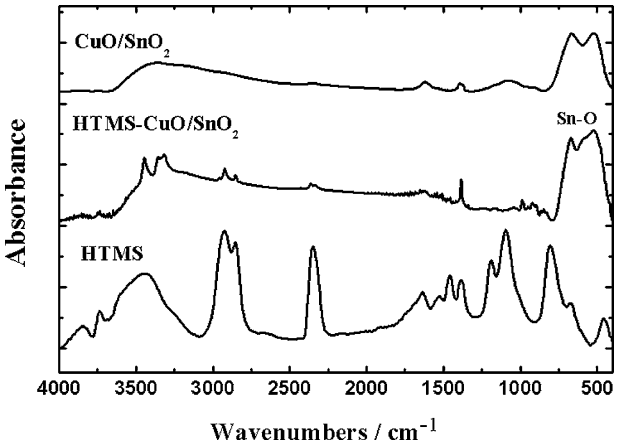

Fig. 4. IR spectrometry of the CuO/SnO_2 mixture, HTMS modified CuO/SnO_2 mixture and pure HTMS.

Sn–O–Sn stretching at 543 cm^{-1} on the CuO/SnO_2 surface occurs. This suggests that the alkyl chains bound to the CuO/SnO_2 surface covalently.

An emulsion polymerization of resorcinol-formaldehyde (RF) was used for in situ coating. Here, we chose resol as a carbon source because resol has high carbon content and can be easily polymerized at 80 °C. In addition, a compact carbon layer appears during its carbonization, which is important for our coating procedure. Many reported studies have failed to synthesize core–shell, carbon-coated, nano-sized, alloy particles, which suggests that without surface modification and appropriate carbon sources, only micrometer intermetallic materials with a high carbon content of more than 40% can be obtained after calcination [15,17].

As mentioned above, the theoretical reduction temperature is affected by both kinetics and carbon resources. The real reduction temperature was identified by DSC analyses. Fig. 5 gives the DSC curves of mixtures containing SnO_2/C, CuO/C and SnO_2–CuO/C in N_2. The carbothermal reduction is endothermic in oxide systems. The board endothermic peaks appear at 890 °C, 801 °C and 820 °C, corresponding to the oxide to metal transformation. From the DSC curve, the CuO reduction temperature is 90 °C higher than SnO_2, and CuO seemed more difficult to deoxidize than SnO_2. However, SnO_2–CuO/C unexpectedly reduces at 820 °C, which suggests that, in the presence of SnO_2, CuO is easily deoxidized. This result agrees with previous work by Wang et al. [13]. Considering all the DSC analysis results, the complete reduction of CuO and the conclusion

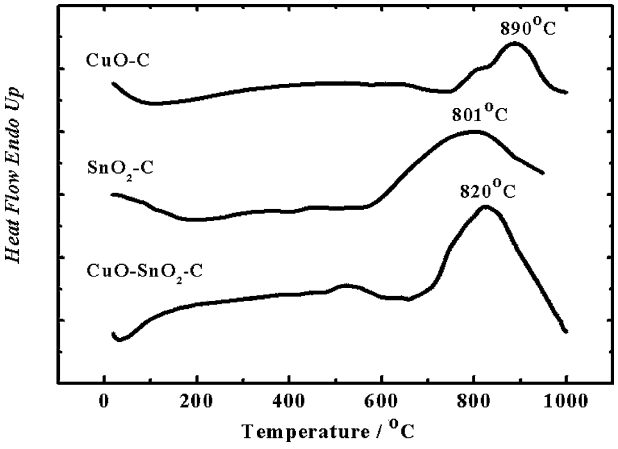

Fig. 5. DSC of CuO/C composite, SnO_2/C composite and CuO–SnO_2/C. The reduction temperatures were identified as 890 °C, 801 °C and 820 °C, respectively. Samples were heated at a rate of 10 °C min^{-1} in a flow of nitrogen.

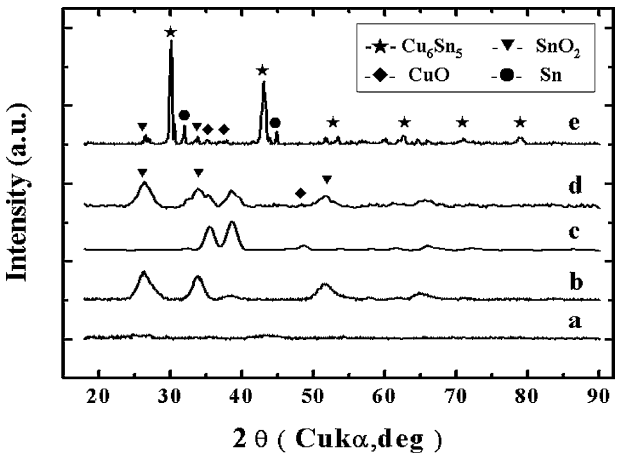

Fig. 6. XRD of (a) RF carbon derived from the carbonization of resol, (b) nano-SnO_2 prepared by hydrothermal method, (c) nano-CuO prepared by thermal decomposition, (d) a mixture of resol-coated SnO_2/CuO and (e) Cu_6Sn_5/C composite.

drawn from the phase diagrams that the treatment temperature should be lower than the alloy formation temperature, we chose the carbothermal reduction temperature for preparing Cu_6Sn_5 alloy to be 900 °C, where carbon has a good electric conductivity. We maintained carbothermal reduction at this temperature for 2 h.

Fig. 6 displays the XRD patterns of (a) RF carbon derived from the carbonization of resol at 900 °C, (b) nano-SnO_2 prepared by hydrothermal method, (c) nano-CuO prepared by thermal decomposition, (d) a mixture of resol-coated SnO_2/CuO and (e) Cu_6Sn_5/C composite. The XRD pattern of RF carbon indicates low crystallinity. In the nano-SnO_2 pattern, we observed peaks at $2\theta = 26.5°$, 33.8° and 51.6°, which are the characteristic peak positions in rutile SnO_2. The peaks were broad and weak due to particle size broadening, which occurs when a sample is made up of very small crystallites. The full-width-at-half-maximum (FWHM) of the diffraction peak can be used to calculate crystallite size using the Scherrer equation:

$$D = \frac{K\lambda}{\beta \cos \theta} \tag{4}$$

From the diffraction patterns, SnO_2 crystallites prepared by the hydrothermal method were determined to be *ca.* 5 nm in diameter, which is highly consistent with the results of the TEM studies. The same information can be found in the XRD pattern of nano-CuO, which shows a typical diffraction of Tenorite CuO with peaks at $2\theta = 35.5°$ and 38.7°. The pattern of the resol-coated SnO_2/CuO before the high temperature treatment shows both SnO_2 and CuO peaks, while the XRD pattern of the treated oxide carbon mixture shows a different diffraction pattern altogether, indicating the formation of a new phase.

The XRD pattern of the final core–shell, carbon-coated Cu_6Sn_5 particles given in Fig. 6 shows a series of large peaks at $2\theta = 30.10°$ and 43° that correspond to Cu_6Sn_5 with a hexagonal NiAs-type lattice structure (*P*63/*mmc*). The high intensity of the main peaks indicates a high crystallinity of the alloy particles and suggests the final product is composed almost exclusively of Cu_6Sn_5, although

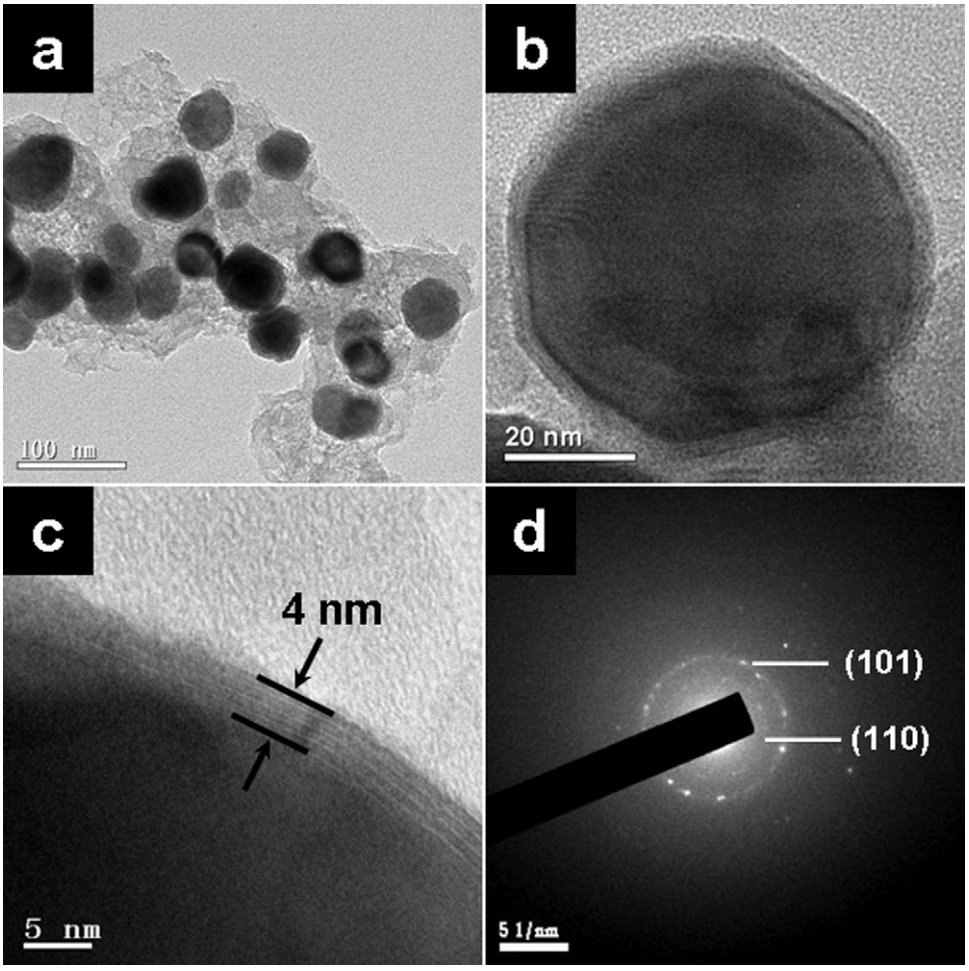

Fig. 7. TEM images and SAED patterns of core–shell carbon-coated nano-sized Cu_6Sn_5.

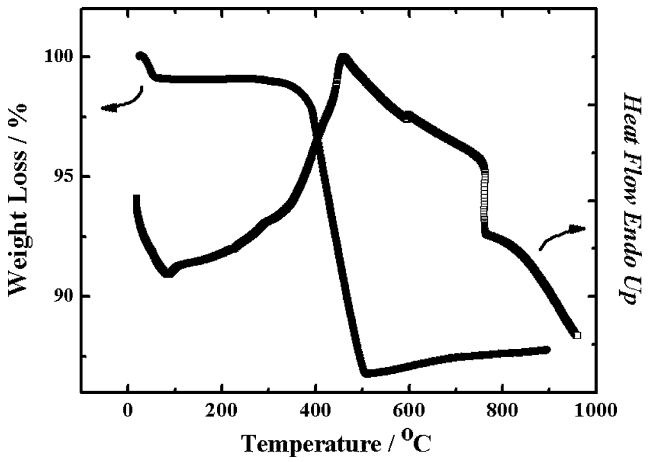

Fig. 8. TG/DTA curves for the core–shell carbon-coated Cu_6Sn_5 obtained in an air flow at a heating rate of 10 °C min^{-1}.

a small amount of another phase (Cu_3Sn) is also present. Further, the average crystalline size of *ca.* 55 nm can be calculated using the Scherrrer formula. Higher X-ray diffraction intensity reveals that the particle size of the carbon-coated sample is larger than that of the oxides precursor (55 nm vs. 5 nm). Other small peaks that appeared in the pattern can be attributed to Cu_3Sn or Sn. The Cu–Sn phase diagram indicates that Cu and Sn can form many intermetallic compounds, *e.g.*, β, γ, δ, ζ, ε and η′-Cu_xSn [22–24]. Cu_3Sn is more thermally stable than Cu_6Sn_5. In our experiment, it is highly possible that an inhomogeneous quenching process gives rise to some other phases and causes the final product to be slightly impure.

TEM images of the final product, Cu_6Sn_5/C, are shown in Fig. 7. The typical size of these Cu_6Sn_5/carbon particles is in the range of 50–60 nm (Fig. 7a). Comparing the results shown in Fig. 2a and c, we can clearly see that the size of the Cu_6Sn_5/carbon composite particles, calcinated at 900 °C for 2 h, is close to the secondary particle size of its precursor. The reductive primary oxide particles aggregate into one particle at high temperature due to their low melting point. It is reasonable to conclude that one secondary aggregate alloy consists of a thousand precursor particles, which shows the possibility of acquiring stoichiometric Cu_6Sn_5 from a nano oxides mixture. The TEM image in Fig. 7b shows typical examples of particles made of a Cu_6Sn_5 core and a carbon shell. A high-resolution TEM image of a selected area shown as an inset in Fig. 7c also clearly reveals that each particle is completely coated by a carbon layer to form a core–shell structure where the carbon shell has been derived from carbonization of the resol shell. The thickness of the carbon layer is about 4 nm. By selecting the desirable carbon precursor and modifying the surface with an in situ polymerization process, the carbon shell effectively prevents the low melting point alloy from pouring off during high temperature treatment, which typically occurs in carbon coating processes for low-melting point Sn alloys, and also makes it possible to keep the alloy particle size in the nano-range. The SAED pattern shown in Fig. 7d indicates clear diffraction rings corresponding to the (1 0 1) and (1 1 0) planes of hexagonal NiAs-type Cu_6Sn_5. They give direct evidence of the composition of the core in our composite. This result also agrees well with the XRD patterns.

Fig. 8 shows TG/DTA curves for the core–shell carbon-coated Cu_6Sn_5 obtained in an air flow at a heating rate of 10 °C min^{-1}. At 500 °C, a sharp endothermic peak appears. This is attributed to oxidation of the carbon layer. The broad endothermic peak from 500 °C to 900 °C corresponds to oxidation of Cu_6Sn_5, which occurs at relatively high temperatures. Only CuO and SnO_2 remain after the RF resin oxidized to CO_2. A carbon content of *ca.* 30 wt% was calculated based on the initial and final weights of the sample, according to the equation given by Wang et al. [13]. The higher tin alloy content, as well as the thinner carbon coating, greatly contributes to the enhanced material performance because the lithium storage density in tin alloy is much higher than that in carbon.

3.3. Electrochemical properties of the Cu_6Sn_5/C composite prepared by carbothermal reduction

It is expected that the core–shell structure of carbon-coated alloy particles prepared by the carbothermal method described

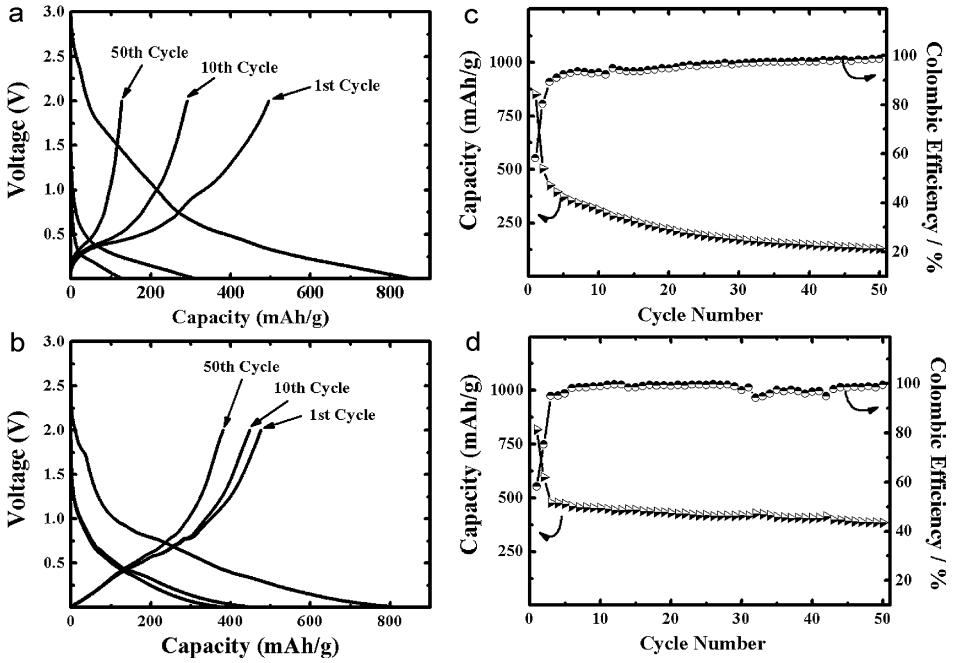

Fig. 9. Charge/discharge profiles for (a) nano-Cu_6Sn_5 prepared by the $NaBH_4$ reduction method and (b) core–shell carbon-coated nano-sized Cu_6Sn_5 recorded with a constant current density of 100 mA g^{-1} between 0.0 V and 2.0 V. The cycleability and coulombic efficiency curves of (c) nano-Cu_6Sn_5 prepared by the $NaBH_4$ reduction method and (d) core–shell carbon-coated nano-sized Cu_6Sn_5.

above would exhibit a good electrochemical profile as an anode material for lithium ion batteries. For comparison, the electrochemical performance of nano-scale Cu_6Sn_5 prepared by the $NaBH_4$ reduction method and the Cu_6Sn_5/C composites were tested in combination with a metallic lithium negative electrode under identical conditions by cycling the cells between 0 V and 2.0 V at a constant current density of 100 mA g^{-1}.

Fig. 9a is the charge/discharge profiles of nano-scale Cu_6Sn_5, which shows a sloping discharge/charge behavior with an initial discharge capacity of 852 mAh g^{-1} and charge capacity of 475 mAh g^{-1}. However, this material exhibits poor cycling performance. The capacity and coulombic efficiency versus cycle numbers are plotted in Fig. 9c. Nano-sized Cu_6Sn_5, without carbon coating, delivers a capacity of only 130 mAh g^{-1} and shows a 74% loss from the first charge capacity after 50 cycles, which is caused by the aggregation of nanoparticles during subsequent cycling. The coulombic efficiency of nano-sized Cu_6Sn_5 rises from 56% in the first cycle to 98% in the 50th cycle, which indicates that the irreversible capacity from the formation of a large amount of surface electronic interface (SEI) film mainly affects the first cycle. This is due to the large surface area of the nanoscale material and the reaction with functional groups existing on the particle surface after the low-temperature synthesis process [6]. The decay of other cycles is attributed to alloy aggregation and pulverization.

Core–shell carbon-coated Cu_6Sn_5 exhibits improved electrochemical performance. As shown in Fig. 9b, several short plateaus in the discharge–charge curves were clearly observed. This can be attributed to the Li–Sn alloy–dealloy process, which agrees with the results reported by Cui et al. [25]. The composite delivers a discharge capacity of 817 mAh g^{-1} and a reversible capacity of 475 mAh g^{-1} in the first discharge/charge cycle, corresponding to a coulombic efficiency of 58% as shown in Fig. 9d, which is not better than that of its competitor. As the composite contains 30 wt% of carbon, the estimated irreversible and reversible capacities contributed by the carbon are about 300 mAh g^{-1} and 90 mAh g^{-1}, respectively. The irreversible and reversible capacities of the pure carbon from the resol precursor during the first charge/discharge cycle are 700 mAh g^{-1} and 300 mAh g^{-1}, respectively [12]. The Cu_6Sn_5–carbon composite delivers a reversible capacity of 490 mAh g^{-1} based on pure Cu_6Sn_5, which is close to its theoretical capacity, assuming that lithium-ion insertion into Cu_6Sn_5 gives rise to $Li_{4.4}Sn$ and Cu. After a deduction of the irreversible arising from the carbon-shell, the columbic efficiency of pure Cu_6Sn_5 within the core–shell structured composite should be 75%. This further indicates that nano-sized Cu_6Sn_5 is full coated by carbon layer, and thus the SEI film mostly forms on the carbon layer rather than on the alloy surface. Core–shell carbon-coated Cu_6Sn_5 demonstrates a good cycling stability compared to that of the nano-sized Cu_6Sn_5. It keeps a capacity of 383 mAh g^{-1} after 50 cycles with a capacity retention maintained above 80%.

As discussed in many works, the carbon-coated nano-alloy shows dramatic electrochemical improvement, especially in cycle stability [8,10,12]. In summary, these improvements could be attributed to three reasons. First, the nano-scale size of alloy particles reduces the lithium diffusion length to a few nanometers. Second, the carbon coating acts as an electronic conductor and ensures good electrical contact during Li insertion/extraction processes. Third, the nano size of the particles limits the absolute volume change of the alloy, so the carbon coating layer has enough mechanical strength to act as a structural buffer, preventing disintegration and aggregation of alloy particles [25].

4. Conclusions

In summary, we developed a modified carbothermal reduction process to prepare a core–shell structured, carbon-coated, nano-scale, Cu_6Sn_5 that uses the precursors of mixed nano-sized metal oxides. The as-prepared composites integrate the merits of intermetallic compounds and nano-sized anode materials. Although the material shows low initial coulombic efficiency, it exhibits an excellent electrochemical performance with higher reversible capacities and improved capacity retention. Carbon-coated Cu_6Sn_5 delivers a reversible capacity of 420 mAh g^{-1} at a constant current density of 100 mA g^{-1} between 0 V and 2.0 V (vs. Li^+/Li), with a capacity retention of 80% after 50 cycles. This improvement in cycling stability could be attributed to the fact that the well-coated carbon layer effectively prevents the encapsulated, low melting point alloy from out-flowing in a high-temperature treatment process. Aggregation and pulverization of nano-sized tin-based alloy particles during charge/discharge cycling is prevented as well. It can be expected that the technology described in the present work can be used to prepare various carbon-coated low-melting point binary alloy nanoparticles and has a wide application in mass synthesis of nano-sized alloy anodes.

Acknowledgements

This work was partially supported by the National Natural Science Foundation of China (No.20633040, 20925312), the State Key Basic Research Program of PRC (2007CB209703), and Shanghai Science & Technology Committee (09XD1400300, 08DZ2270500).

References

[1] A.S. Arico, P. Bruce, B. Scrosati, J.M. Tarascon, W. Van Schalkwijk, Nat. Mater. 4 (2005) 366.
[2] P.G. Bruce, B. Scrosati, J.M. Tarascon, Angew. Chem. Int. Ed. 47 (2008) 2930.
[3] J.M. Tarascon, M. Armand, Nature 414 (2001) 359.
[4] M. Yoshio, H.Y. Wang, K. Fukuda, Angew. Chem. Int. Ed. 42 (2003) 4203.
[5] K.D. Kepler, J.T. Vaughey, M.M. Thackeray, Electrochem. Solid State Lett. 2 (1999) 307.
[6] G. Ceder, Y.M. Chiang, D.R. Sadoway, M.K. Aydinol, Y.I. Jang, B. Huang, Nature 392 (1998) 694.
[7] J.J. Zhang, Y.Y. Xia, J. Electrochem. Soc. 153 (2006) A1466.
[8] J. Hassoun, G. Derrien, S. Panero, B. Scrosati, Adv. Mater. 20 (2008) 3169.
[9] C.M. Park, W.S. Chang, H. Jung, J.H. Kim, H.J. Sohn, Electrochem. Commun. 11 (2009) 2165.
[10] K.T. Lee, Y.S. Jung, S.M. Oh, J. Am. Chem. Soc. 125 (2003) 5652.
[11] W.M. Zhang, J.S. Hu, Y.G. Guo, S.F. Zheng, L.S. Zhong, W.G. Song, L.J. Wan, Adv. Mater. 20 (2008) 1160.
[12] W.J. Cui, F. Li, H.J. Liu, C.X. Wang, Y.Y. Xia, J. Mater. Chem. 19 (2009) 7202.
[13] K. Wang, X.M. He, L. Wang, J.G. Ren, C.Y. Jiang, C.R. Wan, J. Electrochem. Soc. 153 (2006) A1859.
[14] J. Barker, M.Y. Saidi, J.L. Swoyer, J. Electrochem. Soc. 150 (2003) A684.
[15] H.L. Zhao, C.L. Yin, H. Guo, W.H. Qiu, Electrochem. Solid State Lett. 9 (2006) A281.
[16] J. Hassoun, G. Derrien, S. Panero, B. Scrosati, Electrochim. Acta 54 (2009) 4441.
[17] K. Wang, X.M. He, J.G. Ren, L. Wang, C.Y. Jiang, C.R. Wan, Electrochim. Acta 52 (2006) 1221.
[18] C.L. Carnes, J. Stipp, K.J. Klabunde, Langmuir 18 (2002) 1352.
[19] H.M. Xiong, D.P. Liu, H. Zhang, J.S. Chen, J. Mater. Chem. 14 (2004) 2775.
[20] M. Mladenov, P. Zlatilova, I. Dragieva, K. Klabunde, J. Power Sources 162 (2006) 803.
[21] H. Guo, H.L. Zhao, X.D. Jia, X. Li, W.H. Qiu, Electrochim. Acta 52 (2007) 4853.
[22] D. Larcher, L.Y. Beaulieu, D.D. MacNeil, J.R. Dahn, J. Electrochem. Soc. 147 (2000) 1658.
[23] K.X. Wang, M.D. Wei, M.A. Morris, H.S. Zhou, J.D. Holmes, Adv. Mater. 19 (2007) 3016.
[24] Y.Y. Xia, T. Sakai, T. Fujieda, M. Wada, H. Yoshinaga, J. Electrochem. Soc. 148 (2001) A471.
[25] G.L. Cui, Y.S. Hu, L.J. Zhi, D.Q. Wu, I. Lieberwirth, J. Maier, K. Mullen, Small 3 (2007) 2066.